Methods to Fabricate Nanostructures in Stainless Steel to Create Moulds for Nano-imprint Lithography

Andrew Seah[†]

A0110730B

National University of Singapore

Supervisor: A/Prof Jeroen Anton van Kan
Co-Supervisor: Dr Pattabiraman Santhana Raman

A thesis submitted in partial fulfilment for the degree of

Bachelor of Science (Honours) in Physics

2017 April

Abstract

Phase 1 of this project served to fulfill its intended primary objective by investigating and characterising the fabrication of nano-structures in Stainless Steel substrates through means of Ni-masked ion beam lithography. It was found that 2 main factors - namely dose and Ni mask to substrate separation affected the type of structures that can be obtained. For low dose regimes with low mask to substrate separation, an increase in dose leads to an increase in depth and uniformity of structures. However, as the dose increases beyond a critical threshold, redeposition effects, which is the phenomena in which sputtered volumes are reoccupied by material that has been sputtered off, are suspected to hinder further effective sputtering. This effect is complex and likely to be non-linear. A detailed investigation of mask to substrate separation also revealed that Ni mask material deposition in sputtered regions becomes significant if the separation of mask to substrate is greater than 180 μm. Beyond this separation, Ni material is found to be heavily deposited in sputtered areas, effectively impeding the effects of sputtering from achieving greater depths. On the contrary, a separation of less than 100 μm could help greatly reduce this effect.

Phase 2 of this project was motivated because of the desire to investigate closely the redeposition effect with respect to dose, which can only be done if mask deposition effects can be negated. Phase 2 involves creating a mask directly onto Stainless Steel to minimise mask to substrate separation as much as possible. These procedures turned out to be challenging as much calibration is needed. Nevertheless, uniform masks were successfully made onto Stainless Steel surface.

Unfortunately, Phase 2 remains a work in progress and no conclusive results on redeposition effects can be made at this point in time.

Acknowledgements

First and foremost, I would like to express deepest appreciation to my Supervisors - Professor Jeroen and Dr P.S Raman for the opportunity to complete my final year project in Centre of Ion Beam Applications, (CIBA), NUS. Under their guidance, I was able to gather new directions each time experiments seem to have hit a brick wall. This project would not have been possible at all without them, and I am very grateful to them for their unwavering kindness, patience and guidance.

Secondly, credit belongs to my lab mentors and friends - Raj, Tanmoy, Sarfraz, Sumitra, Xin Xi, Liu Fan, Dr Vignesh, Huei Ming, Rudy, Richard Long, Stella, Dan Wei and Ms Ng Soo Ngo for having made this journey an enjoyable, fruitful and fulfilling one. These people have also helped me master operation techniques in many machines available in CIBA & NUS - namely the ISTB, AFM, Nano-Imprinting machine, Spin Coater, UV lithography, Laser Writer, Sputtering Deposition Machine and more. I am indeed grateful to have worked alongside these motivated researchers who have helped in part to fuel my interest in research, and foster CIBA's strong culture of unity.

Last but not least, this thesis marks the end of my formal education (for now), and is dedicated to my loved ones for their unwavering stoic support throughout this hectic period. Their kind understanding and unselfish love has culminated in not only the successful completion of my FYP and undergraduate course in NUS, but also in who I am today. Utmost glory belongs to God for having sustained me and allowing me to achieve all I have today, against all statistically possible odds. The glory is yours, Father. Amen.

Contents

List of Figures

x

1

Introduction

1.1 World of Nanotechnology

Whether we realise it or not, nanotechnology has far reaching impacts in our everyday life. From our anti-reflective glasses[1] to the medical treatment we undergo[2] and even to the anti-stains paint on walls[3] , nanotechnology is at play. More impressively, it has the potential to achieve the things that often appear only on science-fiction shows or in the fig of our imagination. For example, scientists are fiddling with the possibility of creating an invisibility cloak much like the one in Harry Potter and have already achieved success in the microwave optical range thus far[4]. The cloak uses meta-materials with spatially tailored properties that can control the pathways of electromagnetic waves to a high degree. Bullet proof business suits can also be made using carbon nano-tubes which are strong enough to withstand bullets, and yet sleek enough to be worn for business functions[5].

Nanotechnology has indeed ushered in new possibilities, but these possibilities can only be materialised through realising effective methods to create nanostructures. There are quite a number of methods to create nano structures and here is a table showing just some of them.

Methods of fabricating nanostructures can be categorised into two groups: top down and bottom-up. Top down methods involve the progressive removal of material from a larger given material to eventually obtain desired nanostructures. Bottom up methods involve gradually building up structures, starting from the atomic or molecular level, until a desired nanostructure is formed[6]. Bottom

Top Down	Bottom Up
Photolithography	Chemical Vapour Deposition
Scanning Lithography	Molecular Beam Epitaxy (MBE)
Nanoimprint Lithography	Molecular Self Assembly

Table 1 - showing the 2 different categories of fabrication methods of nano material

up methods are often used in the fabrication of simple metal/oxides, polymer elements or self-assembled elements.

1.2 Nano Imprint Lithography (NIL)

Nano Imprint Lithography (NIL) is the method of using a prefabricated mold containing the inverse of the desired pattern and pressing it onto a softer, moldable substrate to yield desired patterns through direct three dimensional mechanical deformation. This molding process is often accompanied by the application of thermal energy or UV rays in thermal and UV NIL respectively. The mold is then removed in a process called demolding, leaving behind the desired features on the substrate[7],[8].

1.2.1 How NIL Compares With Other Methods

NIL is known for its low cost, high speed and high throughput[9], and because it is based on direct mechanical deformation, it is able to achieve higher resolution that is not limited by diffraction limits or beam scattering factors that are encountered in other nanolithography methods. This gives it a promising edge over some methods in terms of resolution and it outshines other methods that can attain high resolution but are too expensive and hence limited to only wealthy faculties. In light of this, NIL has been included in the International Technology Roadmap for Semiconductors (ITRS), and has since been a widely researched field[8].
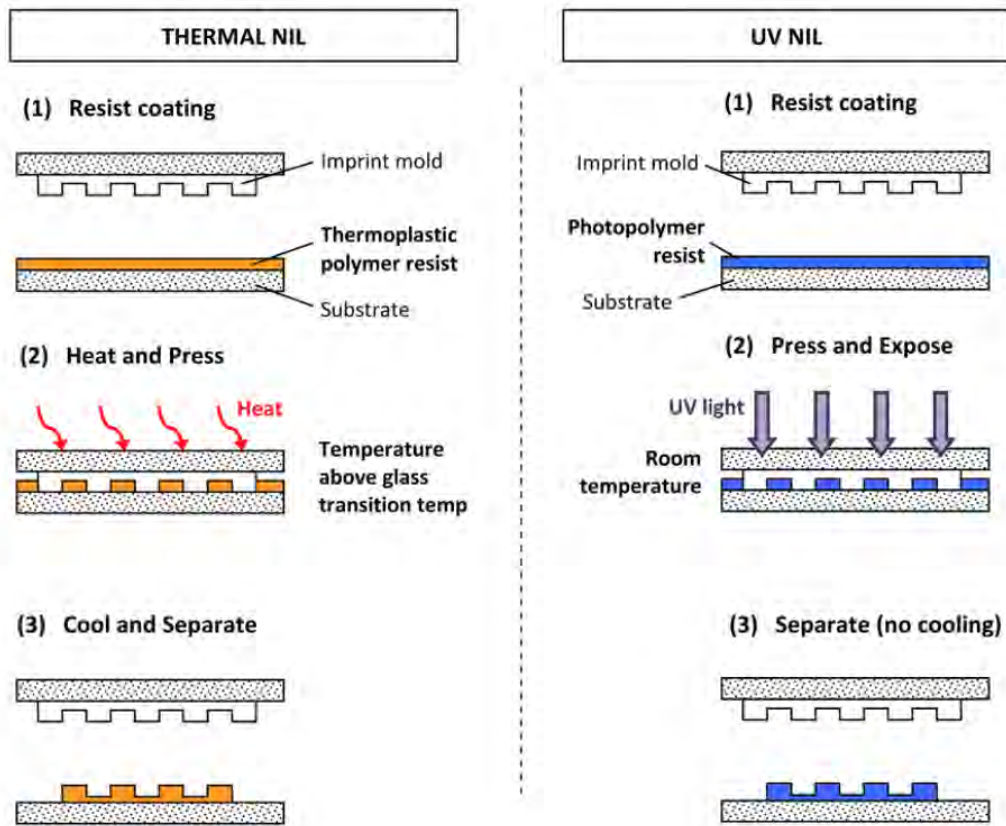
Figure 1.1: Figure showing the general steps involved in Nano Imprint Lithography - Both thermal NIL and UV NIL are depicted. Diagram from Kooy, Review of roll-to-roll nanoimprint lithography, 2014

1.2.2 Disadvantages of NIL

As with any method, there are usually disadvantages associated with it. For NIL, the mold will experience wear and tear, and will eventually have to be replaced. Choosing the right mold with regard to the substrate is therefore essential, because in the process of molding, high pressure is exerted not only onto the substrate but also the mold. Beyond a critical pressure, or if pressure is not applied homogeneously, mechanical damage or even breakage of mold can occur[9],[7]. Furthermore, demolding involves the detaching of the mold from the substrate through a vertical movement, during which structures or designs with high aspect ratio can experience damage more easily[7]. A mold uses the difference in its hardness and the difference in its resistance against stress and mechanical deformation to pattern a substrate. Hence it is essential that a strong mold be used to preserve its lifetime for longer usage.

Silicon is widely used as a mold because of its low cost, decent strength and hardness and also because it can be easily patterned as a master mold using beam sputtering lithography technology[9]. However, more can be done to improve the NIL process by finding a mold that is affordable and yet able to achieve better resolution whilst being more resistant to mechanical damage. This will further improve the attractiveness of NIL as a method to fabricate nano-patterns.

1.2.3 Motivation

Therefore, in this project, we seek to investigate the suitability of an alternative mold that is likely to be able to achieve the same (if not higher) resolution as Silicon while being more resistant to mechanical damage and therefore of a longer lifespan.

Stainless Steel (SS) is one such promising candidate for a mold because it is inexpensive and yet stronger and harder than silicon in many ways as seen in Figure 1.2[10] [11]. The SS used in this project is of grade 304, manufactured by AZOM, and has (17.5 - 20)% Cr and (8-11)% Ni, 2% Mn, 1% Si, and very small amounts (less than 1%) of C, P & S[10] The rest of stainless steel is then made up of Fe. Given its higher strength and hardness, one can expect higher resistance against mechanical deformation and hence a higher expected NIL lifespan. A

Physical Properties of Stainless Steel Vs Silicon		
Physical Properties	Silicon (Adpoted from Almaz)	Stainless Steel (Adopted from Azom)
Bulk Modulus	101.97 GPa	134 GPa
Shear Modulus	79.92 GPa	80 GPa
Young's Modulus	130.91 GPa	190 GPa
Poisson's ratio	0.22	0.265
Hardness	13 GPa	1700 GPa

Figure 1.2: Physical Properties of Silicon vs Stainless Steel - Comparing various physical properties

greater option of softer material including silicon can also serve as substrates to SS molds, therefore opening up new possibilities in the field of NIL. In fact, nano-structures on the SS master mold can be copied onto silicon substrates using NIL too - this not only improves the lifetime of the original SS master mold, but also reduces contamination and damage via direct contact with substrates. In this case, the SS master mold has to house the final desired patterns, so that the silicon intermediate copies will contain the inverse and its subsequent substrates will have the correct patterns[7].

In another paper[12], Schift et al. also rightly stated that a suitable mold for NIL should also have inert chemical properties. Unlike many other metals, SS is able to resist corrosion because of the presence of chromium encoded in its building block. Chromium reacts with oxygen in atmosphere to form a thin passive layer at the atomic scale that prevents further corrosion or reactions[13]. This passive layer not only protects the nanostructures on SS from rusting off, but also from reacting with the substrate chemically even when pressure and thermal energy are applied.

A disadvantage associated with the higher strength and hardness of SS is the increased difficulty in patterning it as a master mold. In fact according to

Schift et al.[12], mold fabrication is one of the biggest hurdles in NIL in terms of achieving high resolution, good uniformity and low defects. Nevertheless, SS is still a material worth looking into with regard to NIL.

2

Objectives

2.1   Primary Objective

The primary objective of this project is to investigate and characterise the fabrication of nano-structures in stainless steel (SS) substrates using ion beam sputtering lithography through Ni mask. Reasons as to why ion beam sputtering was chosen would be explained in further detail in the "Material & Methodology" section.

2.2   Secondary Objective

The problem of redeposition - a phenomenon in which material re-enters volume that was sputtered off, along with how various parameters affect the type of structures obtained, is also investigated.

2.3   Eventual Objective - Beyond this Project

Investigating the effectiveness and suitability of SS as a NIL mold in terms of the resolution of nanostructures that can be replicated onto various substrates and also its durability and lifetime.

2.3.0.1 Convergence of Projects

This project is one of several ongoing projects at the Centre of Ion Beam Applications (CIBA) at NUS, and many of these projects are in reality, part of a bigger project that work towards the same end point. Hence, endeavours to improve the resolution of nanostructures and lifespan of SS mold could be enhanced by applying a diamond-like carbon coating, currently researched on by fellow researchers, Xin Xi (Mr) & Dan Wei (Ms). The diamond-like coating has the potential to improve the resistance of the mold against mechanical deformation and serves to lower the force required in the demolding process, thereby further reducing possible damage to both mold and substrate.

2.3.0.2 Industrial Application

Ultimately, there is hope to introduce SS into the industry as a better alternative hard mold, with actual improvement towards the NIL industry. SS molds could possibly give rise to higher resolution of nanostructures, higher NIL lifespan, and hence lower cost of nanostructures production, improving the methodology of NIL in fabricating nanostructures.

3

Materials & Methodology

3.1 Fabrication Method of Nanostructures on Stainless Steel

3.1.1 Advantages of Ion Beam Sputtering

Table 1 back in the introduction shows various methods belonging to the "top down" and "bottom up" categories. However, not any method can be used to fabricate nanostructures in stainless steel.

For any material to used as a mold in NIL, it needs to be of an acceptable thickness of at least few hundred microns in order to lend strength in pressurising the nanostructures from the mold into the substrate during the molding process. For bottom up methods, this would mean growing stainless steel nanostructures

    i) until they acquire that thickness, or

    ii) upon a flat piece of stainless steel or

    iii) upon some other substrate

The first option is impractical as it takes too long for atoms to be slowly put together till that thickness is obtained, and the second method is both difficult and time consuming to achieve, while the third method results in a deviation from our project's intended eventual objective of assessing stainless steel as an NIL mold.

This leaves us with the top down method, from which we have chosen ion

beam lithography. Ion beam lithography is often closely associated with proton and electron beam lithography, both of which have their advantages, but are unsuitable in this project, for reasons which will be better understood after looking at particle matter interaction simulations and concepts. The decision of choosing ion beam lithography would also be explained later.

3.1.2 Particle Matter Interaction
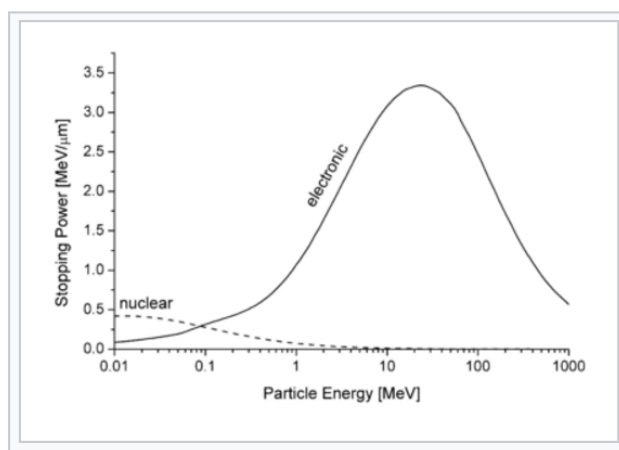
Figure 3.1: Sputtering yield of particles into target in general - Figure shows that 2 main regimes exist - nuclear interaction dominates at lower energy regimes while electronic interaction dominates at higher energy regimes

To better understand how proton, electron and ion beam sputtering works, it would be helpful to first examine particle-matter interaction, which is the study of how particles and matter interact when particles are fired into matter. A particle fired at a target can experience two possible forms of interaction with target atoms - namely Coulomb (or electronic) Repulsion or Nuclear Interaction. Note here, that gravitational interaction of particle and matter is much weaker and can be completely ignored. From the famous Rutherford scattering, it is known that back scattering events (ie. head on nuclear repulsion is very improbable)[14] because the nucleus takes up only 10^{-5} times of the space that an atom occupies, and most of the incoming particles pass through without hitting the nucleus. However, this Rutherford experiment was carried out for a very thin gold foil.

In our case, SS substrate is very much thicker. As such, the argon ions would not pass through the entire substrate. This is supported by SRIM simulations as even argon ions at 20keV could only reach a maximum of around 109 Angstroms. The dominance of the two different interactions mentioned above depends on the energy regime of the incoming ions. In general, nuclear interaction is dominant at lower particle energy regimes whereas electronic interaction is dominant at higher ion energy regimes, as depicted in Figure 3.1. How the particle really interacts with matter also depends on factors such as its mass, and its velocity.

3.1.2.1 Sputtering Yield

Sputtering occurs when particles are ejected from a solid material via **nuclear interaction** when energetic particles are fired at it. This process allows material to be removed from a target, a process often termed as "etching". Energies involved here must of course, be higher than usual thermal energies. The term sputtering yield often refers to the average number of atoms ejected from a target material by each incoming particle fired into it. A higher sputtering yield would mean that more atoms are displaced per unit ion fired, and this corresponds to faster and more effective etching.

Note that the energy shown in Figure 3.2 lies within the energy range order where nuclear interaction is dominant (lower energy range). Within this range, it is shown that sputtering yield initially increases as energy is increased, until a peak is reached. After which, increasing the energy only serves to decrease the sputtering yield. The latter effect is not yet seen for Krypton and Radon but can be observed to some extent for the rest of the particles.

The sputtering yield trend observed can be explained as follows:

The energy of an incoming particle is correlated to the impact it exerts on the target atoms it passes. At very low energies (below the binding energy of a target surface atom), sputtering cannot occur. However, as energy of the incoming particle increases, it exerts a larger force on the atoms that it interacts with, until it finally has sufficient energy to knock out a single atom from the surface (energy loss by ion due to electronic interaction on surface is minimum as compared to in bulk). Imagine firing a rubber band at a stack of partially filled bottles, each time

pulling a little more on the rubber band. The further the rubber band is stretched, the higher its energy. Eventually, the rubber band will be pulled back far enough to be able to dislodge a bottle completely. Similarly, once the incoming particle has energy greater than the surface binding energy of a target atom, increasing its energy increases the chances of sputtering and hence its sputtering yield. However, beyond a certain point, further increasing the energy of incoming ions would only serve to decrease the sputtering yield. This is because of the following competing factor. As the energy of the ion increases, it penetrates deeper into the material. As such, when it loses most of its energy to a particle towards the end of its depth due to nuclear interaction[15], the energy transferred is shared by an cubic increase of atoms proportional to its penetration depth. As such, it is harder for the target nuclei to be sputtered out of the material as they lose most of that energy before they can even emerge from the surface of the target[16].

Sputtering yield also depends on several factors, ranging from the target species to the incoming particle species and energy to its angle of incidence. Because stainless steel is a harder material that requires more time to sputter (compared to silicon), there is hence a desire to choose the parameters that can give us a faster and more effective sputtering yield.

3.1.3 Type of Particle

The next factor to consider is the type of particle that is to be used in for sputtering. Inert gases are highly preferred, to avoid or minimise any chemical alteration or contamination of the target (Stainless Steel) when the ions interact with the target. Hence, nitrogen (because of its strong triple bond) and the noble gases, sit very well with this requirement, along with electrons and protons which are also potential candidates. Figure 3.1 reveal that protons have the lowest sputtering yield compared to any of the ions used. Hence, proton beam lithography to create structures in SS may not be a wise decision.

From Figure 3.1, it is also evident that of the ions considered, Argon fairs much better than Hydrogen, Helium, Neon and Nitrogen in terms of its sputtering yield when compared across energies ranging from 0-20keV. This range of energy is examined because this is approximately the energy range at which ions can
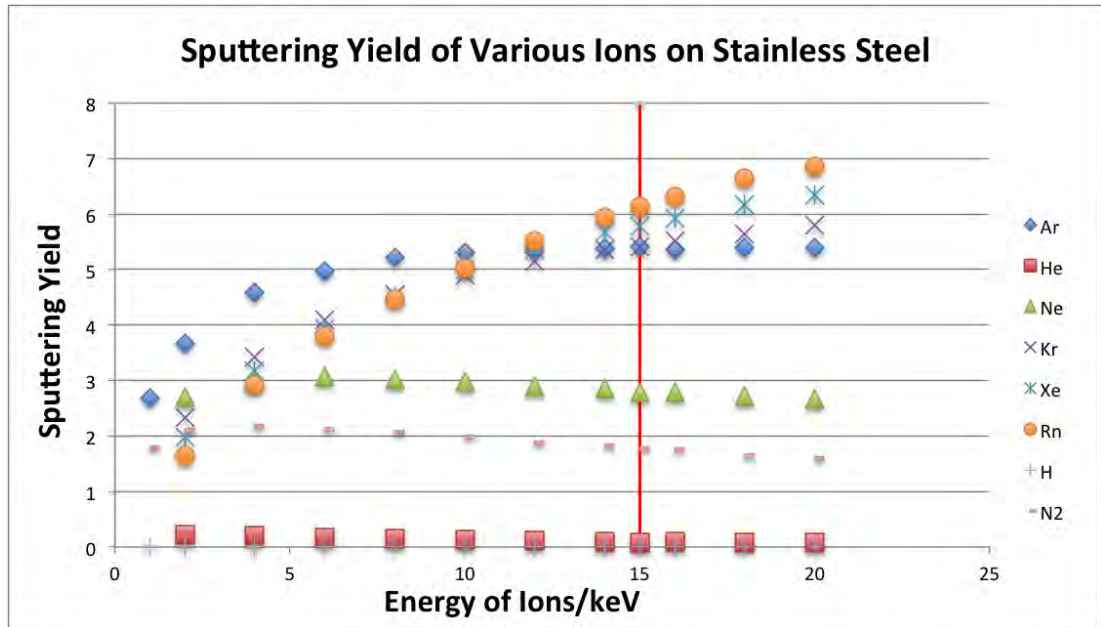
Figure 3.2: Showing the sputtering yield of various ions when fired into stainless steel - Energy range of 1keV to 20 keV investigated

be accelerated to, with the Ion Sputtering Test Bench (ISTB) in CIBA. For simplicity, let us compare the sputtering yield across one energy level - namely 15keV. 3 observations can be made:

(i) 15 keV is the energy for which the sputtering yield of Ar is the highest.

(ii) It is apparent that the heavier the ions used, the higher the sputtering yield.

(iii) However, the increase in sputtering yield diminishes as we proceed down the noble gas group. There is a relatively significant increase in sputtering yield from Helium to Neon and to Argon but significantly smaller increase in sputtering yield from Argon to Krypton, Xenon and Radon.

Taking other practical factors such as availability and cost into consideration, Argon gas is finally chosen.

3.1.4 Mask for Stainless Steel

A suitable mask for Stainless Steel would be one that can fulfill the following requirements:

i) the mask must be able to contain the nano patterns we intend to etch onto the Stainless Steel using Ion Beam Sputtering

ii) the mask must not be etched away before the desired height of nanostructures on Stainless Steel is obtained

Fulfilling these 2 requirements would qualify the material as a suitable mask. From Figure 3.2, the sputtering yield of Ni is 6.2 compared to SS of 5.4. In our case, we have chosen to use nickel mask as it has the next lowest sputtering yiel compared with SS. A relatively thick (5 μm) Ni mask is more than sufficient as we aim to sputter off no more than hundreds of nano meteres of SS with Argon ions at 15 keV.
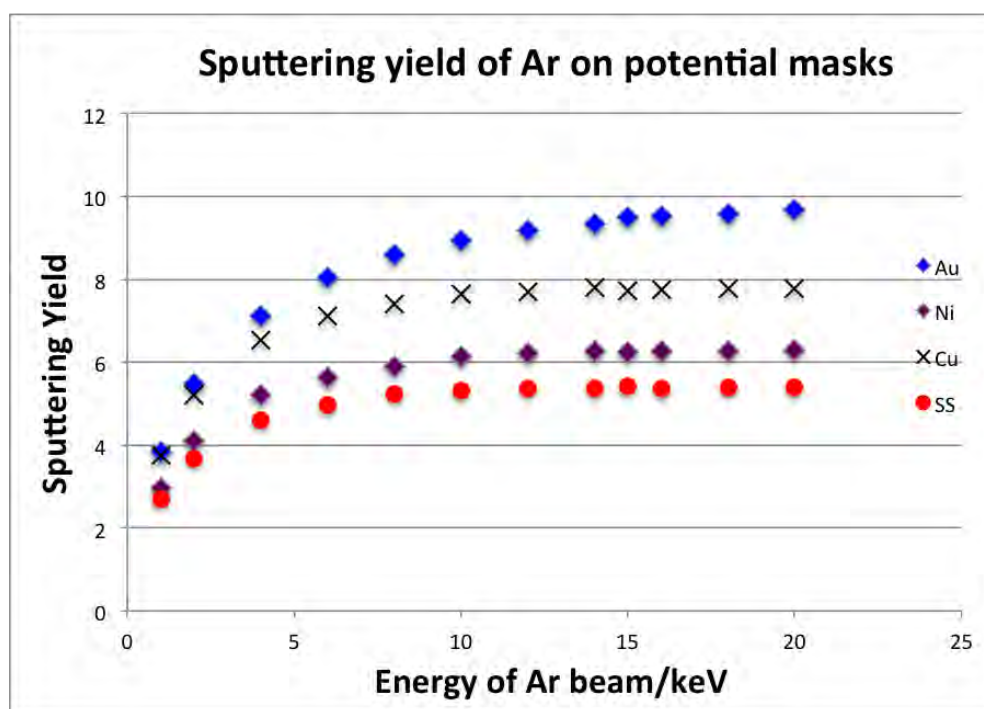
Figure 3.3: Showing the sputtering yield of Ar ions when fired into various potential mask material - Energy range of 1keV to 20 keV investigated

These nickel grids of thickness 5 μm[17] have square holes of 6 μm by 6 μm and the holes are spaced 12 μm apart as labelled in Figure 3.3, a microscopic picture of the Ni Grid. As this project primarily serves to characterise the structures etched onto Stainless Steel by means of ion sputtering, it focuses on first achieving nano-
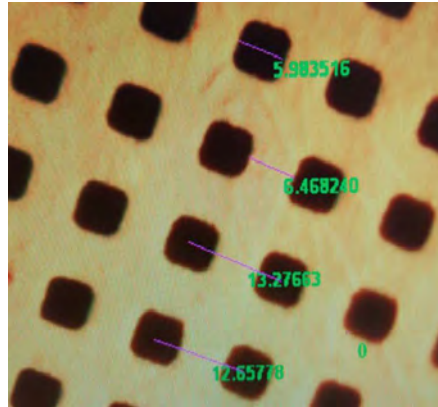
Figure 3.4: Showing the Ni mask when viewed under the optical microscope at 100x magnification - The relevant dimensions have been measured using a microscope analysis software.

depth structures whilst investigating possible redeposition effect, before going on to achieve nanoscale structures in 3 dimensions.

4

Procedures

4.1   Overview of Procedures in Phase 1
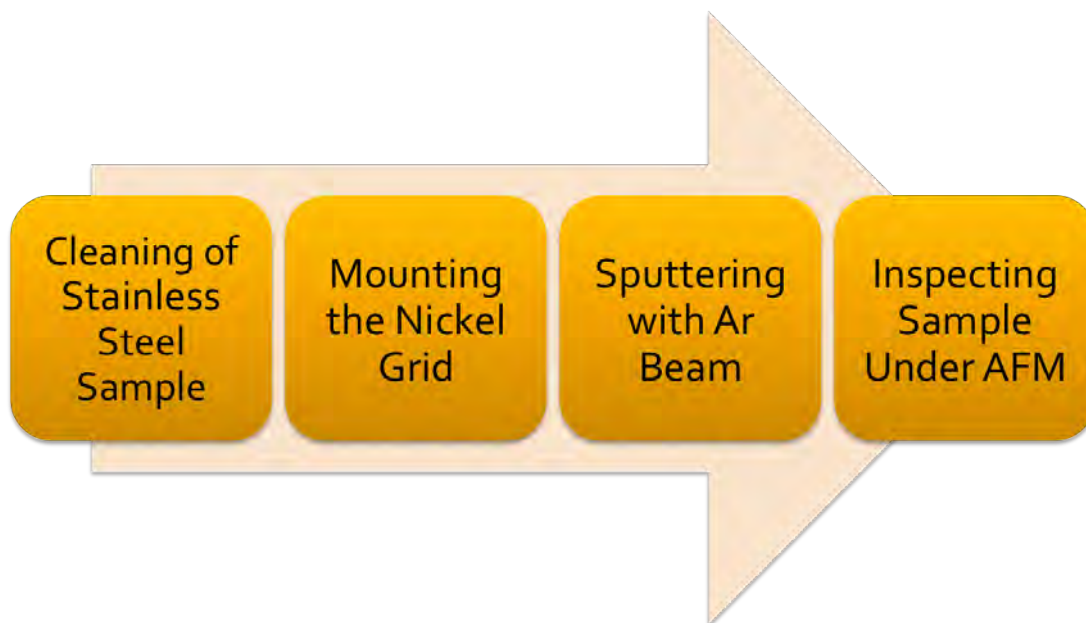
Figure 4.1: An overview of procedures in Phase 1 - Step 2 turned out to especially important as will be elucidated in later sections

4.1.1 Cleaning of Stainless Steel Sample

Each Stainless Steel (SS) sample was first thoroughly cleaned before usage. The cleaning process involves first peeling off a protective adhesive layer, before using lint-free cloth and acetone to gently wipe its polished surface. The SS sample was then placed in a beaker of Isopropyl alcohol which was then treated with ultrasound (35,000 Hz) for 15 minutes at 60° C. The ultrasound causes the SS to vibrate at high frequencies. Coupled with the thermal energy supplied, the particles on the surface of the SS have enough energy to detach themselves from the SS surface, leaving a clean surface behind. The SS is then dried using Nitrogen gas before it is placed into a clean container.

4.1.2 Mounting of Nickel Mask

The next step would be to mount the nickel mask, which is one the most challenging yet crucial process in this experiment. It is challenging to mount the thin sheet of nickel mask flatly onto the stainless steel without causing any crease or tear in it, and yet it is important to do so as will be elucidated in later sections.

Hence, different methods were tried and tested throughout this experiment to achieve conformal, levelled fixture of Ni onto SS. Method 1 involves pinning one end of the nickel mask onto the SS sample using copper tape, before the other end was attached to a second copper tape. The second copper tape was then gently pulled to exert tensile stress on the Ni mask, before adhering it onto the SS. This method proved to be unsatisfactory, because of several reasons:

(i) It was difficult to achieve conformal, levelled fixture because sometimes, creases on the Ni mask or gaps between the Ni mask and the SS can even be observed even with the naked eye. This was later discovered to have a drastic effect on the type of structures obtained after sputtering.

(ii) As the Ni mask is very thin (5um), it tears very easily when under stress and once it is torn, it can no longer be used.

(iii) Tough glue stains are left behind when the copper tapes are removed, making the localised area unsuitable for further experimenting.

The 2nd method of mask mounting uses this method as shown below.

Copper Tape
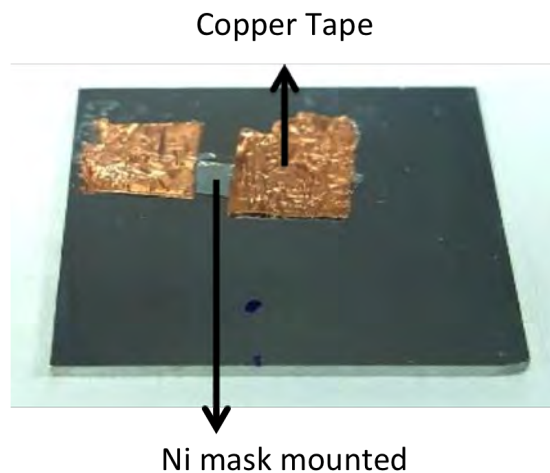
Ni mask mounted

Figure 4.2: Mask Mounting Method 1 - Using copper tape to tape down 1 end first, before the 2nd end of Ni mask is taped down. Here a little gap can be seen between the Ni mask and the SS

Adhesive Tape with aperture

Ni mask below

Figure 4.3: Mask Mounting Method 2 - First cutting a tiny aperture in adhesive tape before a strip of Ni mask is stretched across the aperture pasted down onto the sticky side of the tape. The entire tape is then stretched and pasted onto SS

A small aperture of diameter ~ 3 mm is first cut into an adhesive tape, and the nickel mask is placed across the aperture, before the whole tape is carefully pasted onto the stainless steel sample. This method is thought to be slightly better as tension can supposedly be applied to the nickel mask from all directions. However, in reality, the application of small and equal tension on each side is extremely difficult, even with the help of a colleague. Furthermore, the delicate nickel mask still tears very easily under tensile stress.

Adhesive Tape with washer below

Ni mask mounted

Figure 4.4: Mask Mounting Method 3 - First cutting a tiny aperture in adhesive tape, before placing a metallic washer on the underneath, around the aperture. A strip of Ni mask is stretched across the washer in one direction first, before the entire adhesive tape is stretched along the other direction and pasted onto the SS

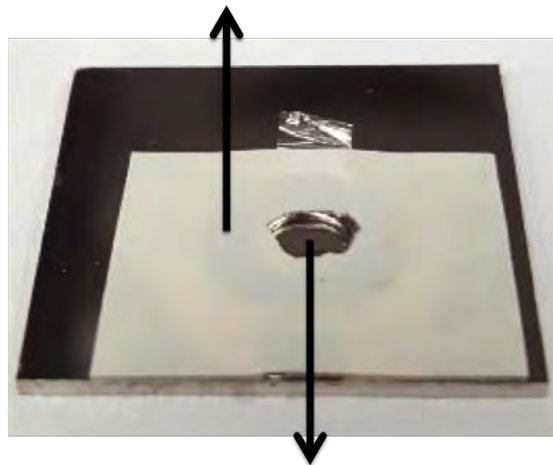Eventually, this method was further improved and modified into mask mounting method 3. The adhesive tape is first flipped such that the sticky side is facing up. A small circular metallic washer is then placed onto the adhesive tape, just around the aperture. A small strip of Ni mask is then gently stretched across the washer and then pasted down onto the adhesive tape. This step allows for tensile stress to first be applied along the length axis. Tensile stress across the breadth is

applied when the adhesive tape itself is stretched along the breadth axis of the Ni mask and then pasted onto the stainless steel. Dividing the application of tensile stress on the Ni mask into 2 separate steps, is thought to make it easier to ensure the Ni mask is pasted on with more isotropic tensile stress and less significant creases. This has helped achieve better conformal fixture and the addition of the washer has reduced tearing of the Ni mask even upon removal, allowing it to be recycled for subsequent experiments.

Figure 4.5: Mask Mounting Method 4 - MMM3 but with added tapes below to help adjust the tension on the Ni mask even after the mask has been mounted onto SS.

4.1.3 Sputtering with Ar$^+$ Beam

4.1.3.1 Ion Sputtering Test Bench (ISTB)

A small gas chamber connected to an RF source, sits at the top of the ISTB. The column beginning with the RF source all the way down to the target is sealed and kept at vacuum levels of approximately 1E-6 mbar. To begin, the gas chamber is first filled with argon gas to approximately 8E-6 mbar, before an RF voltage of ($\sim$100MHz) is applied, causing plasma to be formed. The vacuum level is then appropriately lowered while maintaining a stable plasma. The argon ions
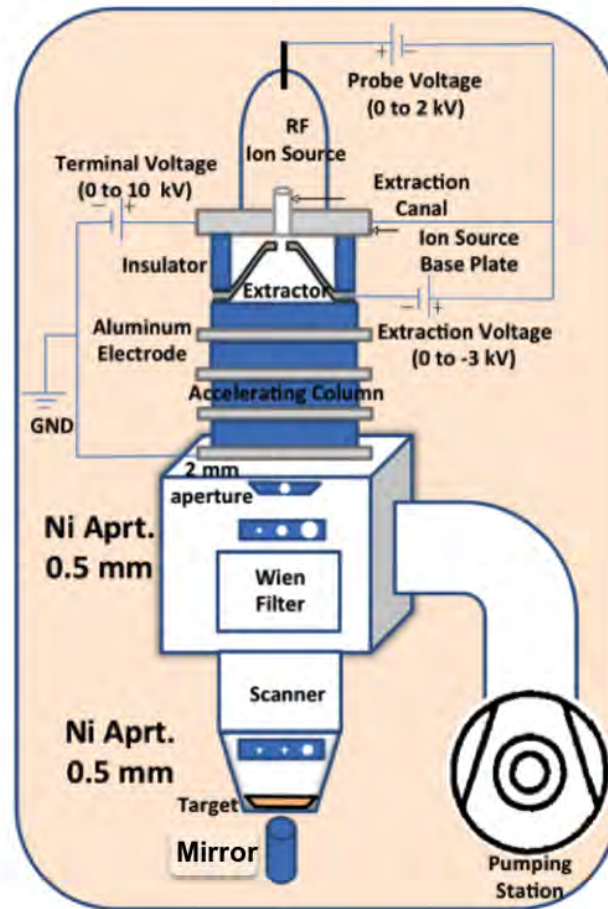
Figure 4.6: Schematic Diagram of Ion Source Test Bench (ISTB) - Diagram shows the set up of the ISTB with the RF ion source, accelerating column, wien filter, apertures kept under vacuum.

4. PROCEDURES

within the plasma are then extracted through the extractor which can be biased at a negative potential as low as -2kV. They pass through the extraction canal into the accelerating column where they are accelerated to the desired energy of 15 keV. The accelerated ions are then collimated through a nickel aperture of 2mm diameter before passing through a Wien Filter which allows only ions with selected energy to pass through a 0.5 mm diameter aperture before hitting the target. [18][19].

The ISTB, as its name suggests, is a test system, collectively assembled by some researchers at CIBA, and is a very comprehensive machine that allows for many parameters to be varied, which grants us more control over experimental variables but this also means that operating the ISTB is a tricky and complex process as many variables are at play, and therefore numerous errors could also occur at times. If these parameters are not kept relatively constant, it would be challenging to explain why we observe what we see. Hence, even a software was developed by fellow rearchers at CIBA for the ISTB, so that as far as possible, many of these parameters could be monitored and better controlled.
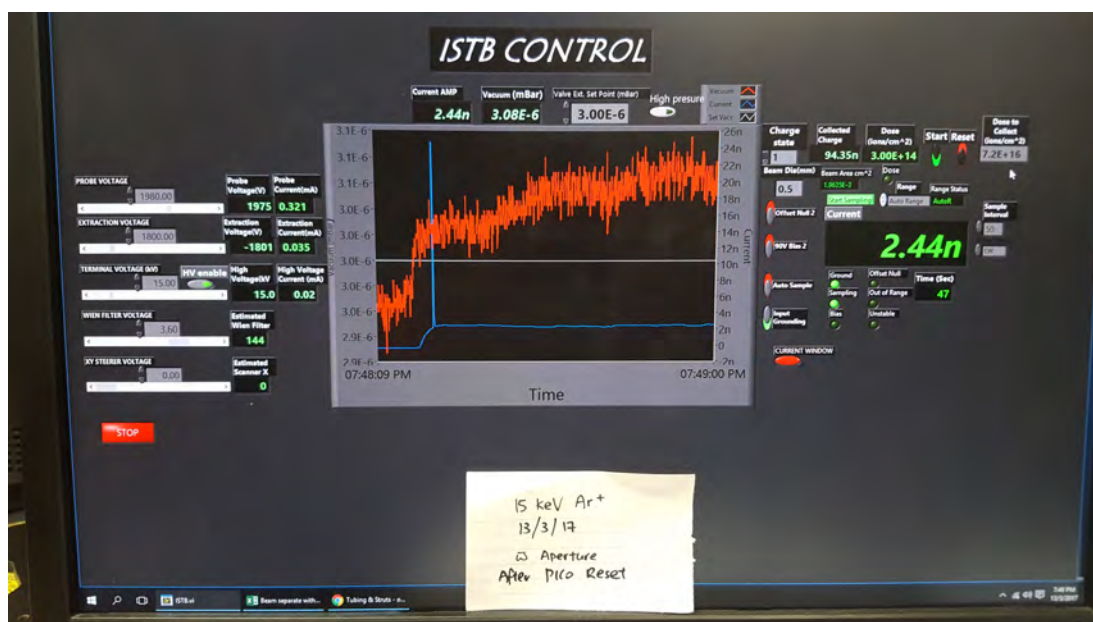

Figure 4.7: ISTB software created by CIBA fellow researchers - Able to track and control probe, extraction, acceleration, wien filter voltages, vacuum levels and more

The entire process of focusing and aligning the ion beam to pass through the final 0.5mm aperture and onto the Stainless Steel sample covered by the Ni mask can easily take up to 4-5 days, because

(i) the beam responds very sensitively to parameters like gas pressure, probe extraction and wien filter voltages. Toggling between these 4 combinations of variables to obtain a focused beam can take up a lot of time as there are many possible combinations. There is also a need to focus the beam as much as possible because if it is too divergent, the proportion of beam that passes through the 2nd aperture will be too weak for etching to be effectively completed within a practical time frame.

(ii) the second aperture has to be manually aligned. Each time any of the above parameters is changed, the beam shifts and the aperture must be likewise shifted. Hence the lower chamber has to be vented and opened so that the aperture can be realigned to fall in line with the beam. The alignment process is done with the help of a theoda light. After alignment, a conductive silver test substrate is placed on the target holder, and the chamber is closed and slowly pumped down to $10^{-6} mbar$. The beam is then switched on once this pressure has been reached, with the parameters set to achieve maximum focus through the aperture. The focus of the beam can be monitored in 2 ways - (1) by checking the current reflected on the software of the ISTB and by (2) the beam spot on the silver test substrate which can usually be observed after some time. A current is registered because argon ions which hit the target causes a net positive charge to be accumulated on the target, which is neutralised by the flow of electrons from the ground into the target. The flow of electrons constitutes to this current and is closely monitored because it is indicative of the amount of argon ions that hit the target per unit time. Maximum current corresponds to maximum proportion of argon beam focused through the aperture and is highly desirable because this means etching can occur more quickly. We are usually able to achieve 2-5 nA at best. At the same time, the beam spot can be used to double-check if focus is indeed achieved. A low current (order of 100s of pA) with a small beam spot (0.5mm in diameter) means that the beam did pass through the 2nd aperture but it is not focused, whereas a high current with a large beam spot means that the beam is so unfocused that most of it falls outside of the aperture onto the target.

4. PROCEDURES

Only when a small beam spot and a relatively large current (of the order of nA) is obtained, can we be sure that the beam is decently focused and aligned to the 2nd aperture.

(iii) Pump-down time to pressure of 1E-6 mbar which is necessary before experiments can proceed, takes approximately 4 hours.

4.1.3.2 Sputtering Process

Once the Ni grid is attached onto the SS, it is loaded into the ISTB where Ar ions are fired at the sample. Ar ions are accelerated to 15 keV before colliding into the sample, because highest sputtering yield is obtained at that energy level according to earlier SRIM simulation done in the energy range of 0-20keV. The software on ISTB is able to keep track of the dosage obtained, by means of the following formula:

$$Dosage, D(ions/cm^2) = \int_0^T (I/qA)dT \qquad (4.1)$$

Here, T represents the total time elapsed (in seconds), I refers to the instantaneous current at any point in time (in amperes), q is the charge associated with each ion (in Coulomb), and A is the area of irradiation in cm^2.

$$d(cm) = (D * Y)/\rho \qquad (4.2)$$

The expected sputter depth, d (in cm) can be obtained from equation (4.2), in a simplified model that does not take into account redeposition effects nor incident beam that hits the surface at an angle, both of which would serve to lower actual sputter depth obtained. Nevertheless, equation (4.2) is useful in helping us gauge the theoretical values of sputtering depth that can be obtained, whilst giving us hints on how significant redeposition effect is in our experiments. D is the dosage in (ions/cm^2), Y is the sputtering yield obtained from SRIM simulation which depends on the species of incoming particle, its specified energy and the type of target material. ρ refers to the atomic density of the target material, in our case, that of stainless steel.

The ion beam sputtering process is usually closely monitored as many things can go wrong. For example, the power supplies may overheat and malfunction,

cutting supply of the Ar ions, or the mass flow controller could malfunction, causing argon gas pressure to rise rapidly, thereby leading to damage in the turbo air pump if not quickly remedied. Operating the ISTB is indeed a tricky process, but mastery of this machine which includes prompt fixing problems when they arise was achieved through experience and guidance from colleagues. A standard operation procedure (SOP) has also been created through this project for future users of the ISTB.

4.1.4   Inspecting Sample Under AFM

After the sputtering process is completed, the sample can be examined under the Atomic Force Microscope (AFM) to understand its surface morphology.

4.1.4.1   How AFM Works

In AFM, a sharp probe attached onto a cantilever is made to run across the surface. The localized mechanical interaction between the probe and the sample surface causes the cantilever to experience bending. A laser beam reflected from the backside of the cantilever into an optical sensing system with a quadrupole photodiode array is used to monitor this bending very accurately. The vertical displacement due to normal forces or the lateral twist due to friction forces is detected and processed based on the relative light intensity detected by the 4 diodes. A feedback mechanism is also used to maintain a constant tip-sample distance during imaging. For this project, the tapping mode of AFM was used, to help reduce tip/sample damage. The AFM provided in NUS is able to achieve a high resolution of 0.1 nm.

4.1.5   PHASE 2

Phase 2 was kick-started despite the severe time constraint due to the fact that the project was about to end, because there was a strong desire to investigate more closely how grid distance (from the substrate) and conformity affected the type of structures obtained through sputtering (see Results Phase 1). In phase 2, endeavours were made to "grow" a mask directly onto stainless steel. This

4. PROCEDURES

intricate and arduous process involves having to use at least 4 new machines, one new software, many new chemicals, along with much calibration, trial and error, and perseverance at each stage of the process.

The idea of creating a mask directly on SS is met with many possible methods, but also with almost as many constraints given the resources, feasibility and time. At least 3 plausible methods stood despite these constraints and the following segment is used to highlight these methods.

4.1.5.1 Method 1

A thin layer of AZ 1518 ($\sim 1\mu m$), a positive photoresist can first be spin coated onto SS, before it is baked. A chromium mask with suitable patterning was also self-fabricated (elabroated later) and then placed over it, before it was exposed to UV light at 200 W for a 45s. The AZ is then developed using AZ400K which was diluted with distilled water in the ratio of 1:4. Once developed, the SS sample is then sputtered with a very thin layer of chromium (approximately 10 nm) before it is then sputtered with 500 nm of copper. The purpose of the thin layer of chromium serves as an adhesive which allows copper to be attached onto it so that easy lift off via chromium etching can be achieved when we wish to remove the entire mask after sputtering. Next, remove the AZ using acetone, and this leaves only the mask pattern of Cr and Cu on the SS. The sample is then sputtered with Ar ions at 15keV, and the Cr etched off after the entire sputtering process. Finally, the SS would then be examined under the AFM.

4.1.5.2 Method 2

Another method involves first coating the entire SS with Cr (10nm) and then Cu (10-20nm) before coating it with 1um of AZ. The AZ is once again placed under a suitable mask pattern, and then exposed to UV light and developed. Once the AZ is developed, it is electroplated with Ni which would adhere to only the copper surface since copper conducts electricity. AZ is then etched off, followed by copper and then chromium, leaving behind only the Cr/Cu regions that are masked by the Ni electroplated earlier. This method would be a closer parallel with phase 1 in which we also used Ni mask, but this method takes up more time, because

it involves the additional mastery and operation of the electroplating machine, along with proper calibration of 3 separate etching processes. More importantly, the quality of Ni via electroplating can be compromised when plating a very thin layer ($< 1~\mu$m). There could also be a risk that some of the Ni/Cu/Cr pillars are completely wiped out in the chromium and copper etching processes, especially after fellow colleagues have reported that the copper etchant we have is capable of also etching Ni. If successful, the sample, however would likewise, be sputtered with 15keV argon ions before Cr etchant is used again to completely remove the mask.

4.1.5.3   Method 3

Method 3 also serves to draw a closer parallel to Phase 1. AZ of 1-2 μm is first coated onto SS, masked suitably and exposed to UV, before it is developed. Next, a thin coating of 10 nm of Cr and of Cu is coated on. Finally, Ni is electroplated onto the surface. However, since sputtering causes the entire surface including the steps to be covered with a thin layer of Cu, electroplated Ni may be found across the entire surface as well as along the side walls between 2 adjacent Cr/AZ structures. This can potentially cause Ni to be electroplated onto the sidewalls as well, in what is known as step coverage. Step coverage could then cause Ni from the lower step to be peeled off when the Ni on the higher steps are removed by means of AZ removal. This could possibly lead to poor quality and uniformity of mask and could potentially affect our results drastically. Yet, this method has an advantage in that the removal of AZ using acetone would not etch away the Ni/Cu/Cr structures, and also allows for easy removal of these structures after sputtering.

Method 1 was eventually chosen, for its speed and relative ease. Copper material used directly as a mask. Even though it differs from Ni used in Phase 1, is not expected to alter our results in any drastic known manner, especially since its sputtering yield is not too different from Ni. In method 1, 500 nm of Cu is used as a mask in view of its higher sputtering yield when subject to 15 keV Ar beam as compared to Nickel or SS, as seen from Figure 3.2. which depicts SRIM simulation results.

4. PROCEDURES

In the above methods, the use of a self-fabricated chromium mask was mentioned. This mask is designed to resemble the Ni mask used in Phase 1, so that the resulting structures can be more closely compared to that of Phase 1. Autocad, a design software, which is compatible to the laser writer at CIBA, is carefully utilised to create 2 separate designs, one to write off the grids, and one to write off the holes, with similar dimensions to the Ni mask in Phase 1, so that either design could be used as appropriate in each of the fabrication processes. These designs were written onto a piece of glass coated first with chromium and then AZ1518, using a laser writer. Once the topmost AZ resist is written off and developed, the mask was sent for chromium etching before it was inspected under a microscope. Finally, the rest of the AZ was also cleaned off with acetone and the mask is ready to be used in UV lithography.

The above procedures in phase 2 alone granted an opportunity to master various new machines, techniques and software, namely spin coating, developing resists, baking, etching, laser writer, UV lithography and Sputtering Deposition Machine.

5

Results & Discussion

5.1 PHASE I

5.1.1 Results from Mask-Mounting Method 1

In Section 5, different methods of mounting Ni mask onto stainless steel were discussed. In each case, the procedures remain the same. Once the Ni mask is mounted onto Stainless Steel, it is placed into the Ion Sputtering Test Bench (ISTB) and sputtered with 15 keV Ar ion beam. After the desired dose is achieved, the sample is taken out and the Ni mask carefully removed, before the SS is examined under the AFM. Figure 5.1 shows the AFM results obtained when mask-mounting method 1 was used. Two different dosages, namely 3E16 ions cm^{-2} and 3E17 ions cm^{-2} were examined and depicted below.

For AFM height profiling, brighter regions represent higher regions while darker regions represent lower ones. For both doses, similar types of AFM images were obtained. Both have brighter (ie. higher) squarish structures which resemble the squarish holes in Ni mask whereby no nickel material is present to shield against sputtering, while the darker (ie. lower) regions of the AFM image resemble the actual Ni grids that are supposed to shield off the Ar beam.

The heightened structures in the 3E16 dose were found to be (230 ± 20) nm while that of the 3E17 dose was found to be (380 ± 10) nm. The height of these structures were obtained through the use of the "section" function of the AFM Analysis Software. At least 10 such structures were examined for each

Figure 5.1: Height & Phase Profile of 3E16 ions cm⁻² - For Height Profile: Brighter parts refer to higher structures while darker parts refer to lower structures. Phase Profile shows Ni in squarish "holes".
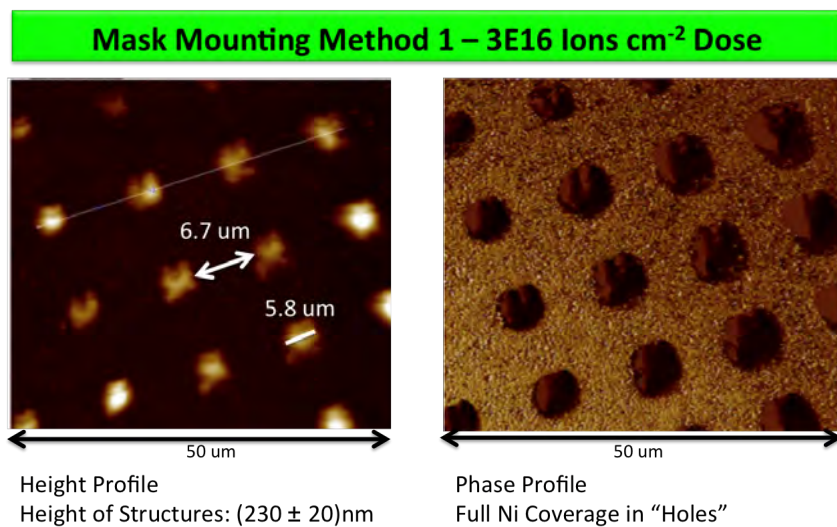

Figure 5.2: Height & Phase Profile of 3E16 ions cm⁻² - For Height Profile: Brighter parts refer to higher structures while darker parts refer to lower structures. Phase Profile shows Ni in squarish "holes".
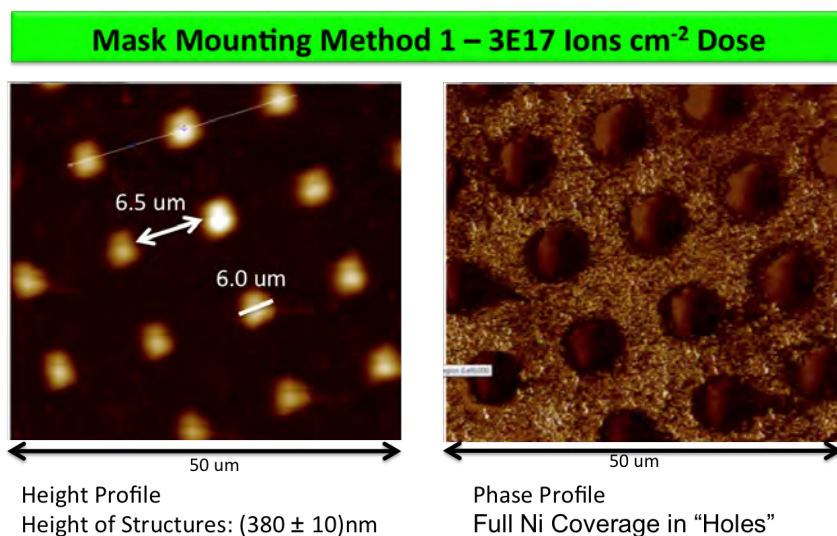
experimented dose, and the average along with the corresponding uncertainty is worked out. An example of how these depths were measured is shown below.
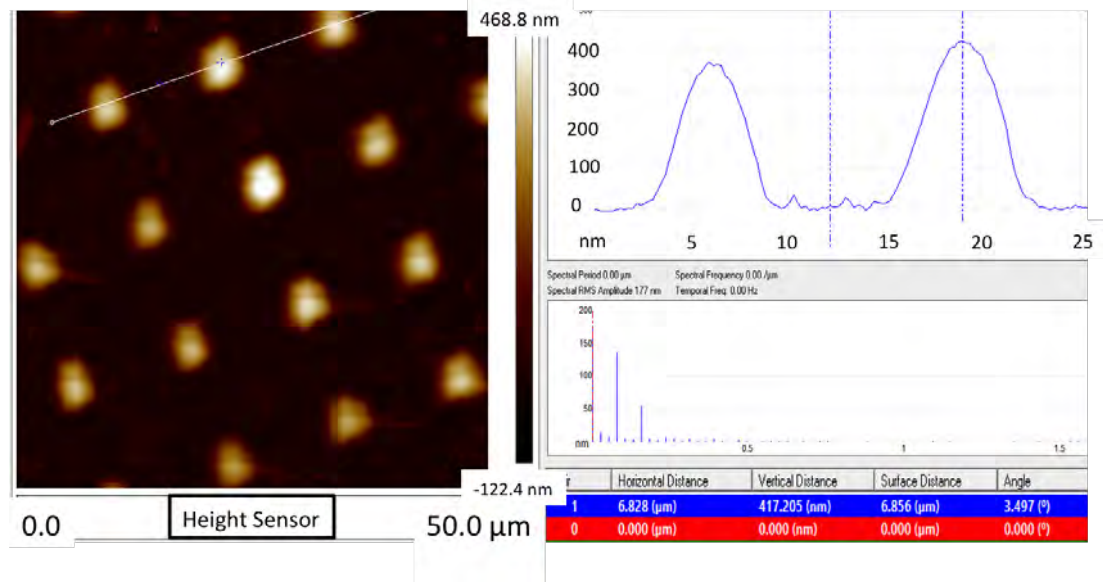

Figure 5.3: Height Profile of 3E17 ions cm⁻² using Mask Mounting Method 1 - 2 points are chosen, one on the SS surface, and the other in the "hole" and the vertical distance is given by the software

5.1.2   Analysis of Mask-Mounting Method 1

These images seem counter intuitive as squarish holes on the Ni mask are expected to allow Ar ions to pass through and sputter off SS material, supposedly creating a depth (which should be depicted as a darker region), while SS regions masked by Ni grids should have been shielded from Ar sputtering, giving rise to relatively higher regions. In other words, the experimental results obtained have contradicted expectations and hence this phenomenon was closely examined and investigated.

The phase images of the above samples were also taken using AFM and studying them actually revealed hints as to why our experimental results were as such. The phase image capability of AFM is able to distinguish material based on their differing stiffness [20], and would depict materials which have different stiffness with different corresponding colours.

5. RESULTS & DISCUSSION

Both phase images above clearly show the squarish regions to be of a darker shade as compared to its surroundings, with clear delineation between them suggesting that 2 different materials exist on this surface - one being stainless steel surface and the other nickel.

5.1.2.1   WHY NICKEL?

There are strong reasons as to why the material introduced onto SS suraface is indeed Nickel, as elaborated below:

(i) It is found evidently in the square regions

The Ni grids on the Ni mask used is at least 10 times thicker ($\sim 5\mu$m) than the depth of material that will ever be sputtered off (order of 100 nm) in our experiments, hence they are never completely sputtered off in any of our experiments. After mounting the nickel mask, the grids create elevated platforms that surround relatively sunken holes which expose the stainless steel (SS) surface below. Incoming argon ions would initially sputter off both stainless steel and Ni. However, the Ni that is sputtered off is likely to fall off randomly, and has a chance of falling into the neighbouring holes. This chance is thought to be more pronounced especially when the grids are not tightly pressed against the stainless steel surface. In fact according to Bartelt, this factor led to a loss in resolution of 0.1 μm even for a 1 75 keV proton beam[21]. As more Ni gets sputtered into these holes, it covers the stainless steel and prevents it from being sputtered further - Ni has a stopping range of just 7 nm for 15keV Argon ions according to SRIM simulations. In some cases, holes are slowly packed with more and more Ni material and can even reach the order of hundreds of nanometer above SS surface, causing the sputtering of SS to reach a complete halt. Eventually, when the desired dose is completed, the Ni mask is carefully removed, leaving behind the "holes" that are now packed with Ni material. As such, these "holes" appear higher than the surrounding stainless steel surface as they have additional Ni on top of the surface, which could indeed explain why we see higher structures in the squarish regions.

(ii) It is not found along the tracks

When Ni grid is removed, 2 things could happen - either it is removed cleanly or bits of it from the underside could be left behind on the stainless steel surface due to strong adhesion. If the latter occurred, the residual is unlikely to have been left behind evenly, especially since it was not placed with perfect conformity onto SS - this will be further substantiated later. Hence, we should expect inhomogeneous shades of colour in the tracks where the Ni grid was removed. Yet, the AFM images clearly show that the track area from which the Ni grid was removed is of a highly homogeneous colour, indicating that the latter was unlikely to have happened. Note that the AFM phase image is capable of imaging phase differences even at the nano scale, but no such apparent differences were observed in the local area, giving reason to believe that the removal of Ni mask was a clean process.

Much effort is then invested towards different nickel mask-mounting processes, because there is clear evidence that the extra material came from the mask during sputtering process, and the amount of Ni material deposited into these holes was suspected to have a correlation to its height from the SS surface and also its conformality. If so, achieving a more conformal and more tightly pressed Ni mask onto stainless steel would reduce the likelihood of Ni being sputtered into these holes.

5.1.3   Results of Mask-Mounting Methods 2 & 3

Hence, the entire procedure of (i)cleaning a new stainless steel, (ii) mounting the nickel mask, (iii) sputtering it with Ar beam and finally (iv) inspecting it under the AFM was repeated, with added emphasis given to step (ii). This time, however, different mask-mounting methods namely 2 & 3 introduced in the Section 4: "Procedures" were invented and employed, and the Ni mask was noticeably flatter and more tightly pressed against the stainless steel as compared to mask-mounting method 1.

The dosages were kept the same as before, so that a fairer comparison could be made across different mask-mounting methods. The figure below shows the images obtained under the AFM.

Height Profile
Depth of structures: (140 ± 14)nm

Phase Profile
SS with Ni boarders in "Holes"

Figure 5.4: Height & Phase Profile of 3E16 ions cm⁻² - For Height Profile: Brighter parts refer to higher structures while darker parts refer to lower structures. Phase Profile shows SS with Ni boarders in "holes".

Height Profile
Depth of structures: (19.8 ± 0.9)nm
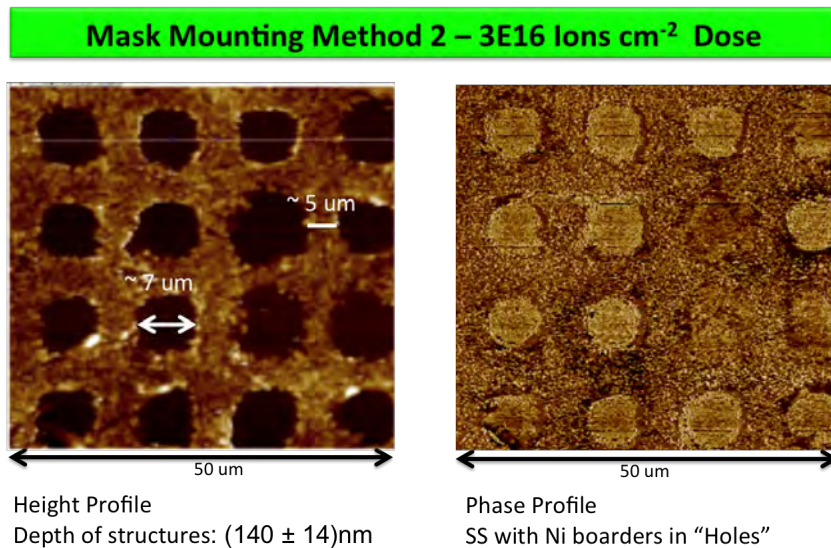
Phase Profile
SS with Ni boarders in "Holes"

Figure 5.5: Height & Phase Profile of 3E17 ions cm⁻² - For Height Profile: Brighter parts refer to higher structures while darker parts refer to lower structures. Phase Profile shows SS with Ni boarders in "holes".
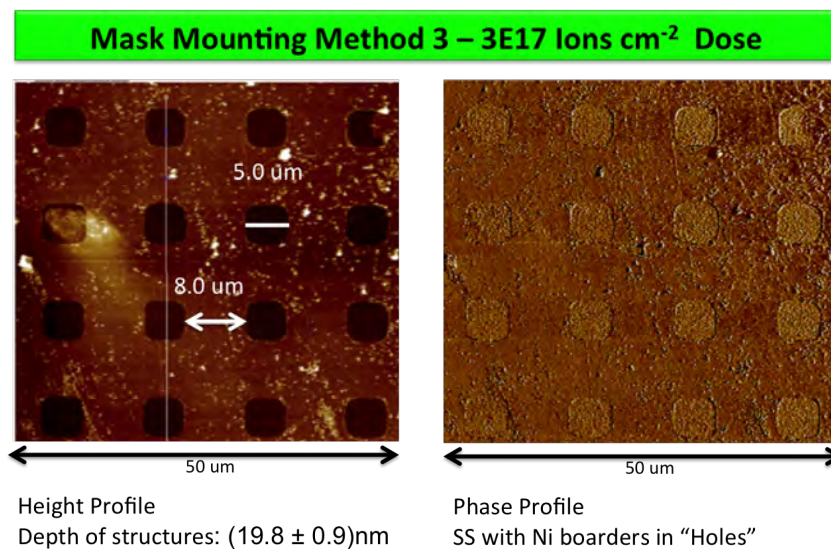
It is apparent that both AFM Height Profile images reveal similar structures to those previously obtained, except that this time, the colours are now inverted - the squarish regions are now of darker shade, representing a lower region, while the grid regions are depicted with a lighter shade, representing a relatively higher surface.

The corresponding phase profiles also show relatively much higher homogeneity in its shades especially for the 3E17 case which corresponds to the mask-mounting method 3.

5.1.3.1 Analysis of Mask-Mounting Methods 2 & 3

The homogeneous phase profiles imply that only one main type of material exist on the stainless steel surface - it could either be completely stainless steel or completely Ni. Again, reason (ii) from earlier section states that if Ni was left behind on the SS after the Ni mask was lifted off, there should be much inhomogeneity in the way it was left behind on the SS surface, but this was not the case. And if Ni grid was indeed well removed, the material left behind on the tracks would be mainly stainless steel. Since the tracks and the squarish areas are of the same material - it is safe to say that the entire surface is stainless steel.

The above results seem to validate the suspicion that mask-mounting does have significant influence on the type of structures obtained. However, it is still too early to comment or draw conclusions at this point in time.

Hence another dose of 3E15 ions cm^{-2} was also obtained, using a new mask made with Ni mask-mounting method 2.

The 3E15 Height Profile shows rather irregular structures that are heightened above the surface. These heightened structures come from the Ni mask, and are only faintly reflected in the Phase Profile.

5.1.4 Results of Mask-Mounting Method 4

To better investigate how the type of structures obtained is related to the dose of ions used, different doses were obtained. Along the way, new mask-mounting methods were tried and tested. Of some of these methods, mask-mounting

Mask Mounting Method 2 – 3E15 Ions cm⁻² Dose

Height Profile
Depth of structures: (2.6 ± 2.8)nm

Phase Profile
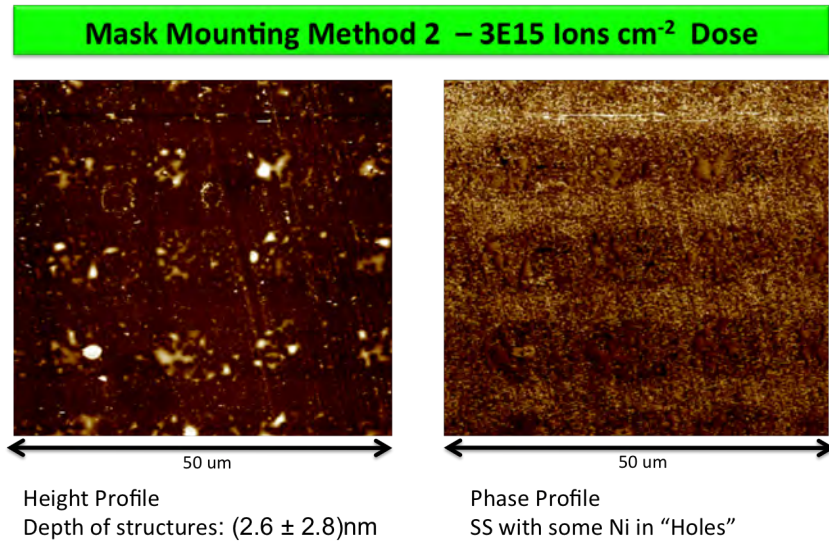SS with some Ni in "Holes"

Figure 5.6: Height & Phase Profile of 3E16 ions cm⁻² - For Height Profile: Brighter parts refer to higher structures while darker parts refer to lower structures. Phase Profile shows partial Ni coverage.

method 4 was thought to be a better one, therefore a dose of 8E15 and 8E16 were taken using this method.

For the dose of 8E15 ions cm⁻², we clearly see a neat delineation in structures in its Height Profile, which clearly resemble the holes and the grids of Ni mask. The same is found for the 8E16 ions cm⁻² dose. The phase images however shows a disparity. For the 8E15 ions cm⁻² sample, it was clear that the holes are SS, just like the rest of the surface, with some Ni material delineating its boarder, but for 8E16 ions cm⁻² sample, the holes were clearly filled up with Ni material, even though the same Ni mask was used for collecting both 8E15 ions cm⁻² and 8E16 ions cm⁻². However, it was clear from the beam spots, that the beam had passed through different parts of the mask).
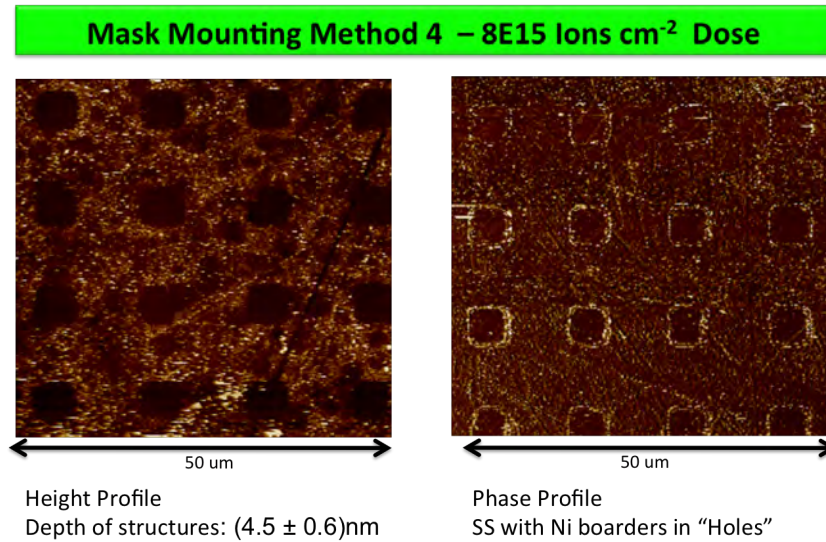
Height Profile
Depth of structures: (4.5 ± 0.6)nm

Phase Profile
SS with Ni boarders in "Holes"

Figure 5.7: Height & Phase Profile of 3E16 ions cm⁻² - For Height Profile: Brighter parts refer to higher structures while darker parts refer to lower structures. Phase Profile shows partial Ni coverage.

Height Profile
Depth of structures: (8.1 ± 0.8)nm

Phase Profile
Full Ni Coverage in "Holes"

Figure 5.8: Height & Phase Profile of 3E16 ions cm⁻² - For Height Profile: Brighter parts refer to higher structures while darker parts refer to lower structures. Phase Profile shows partial Ni coverage.
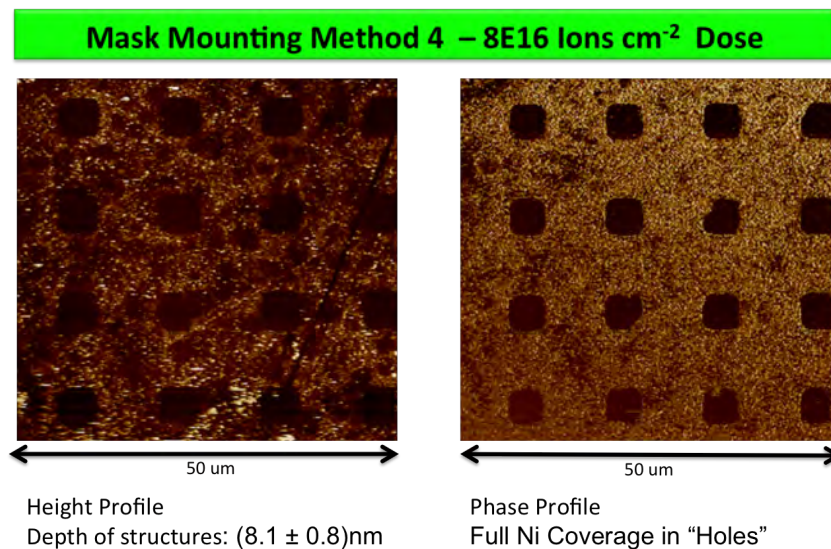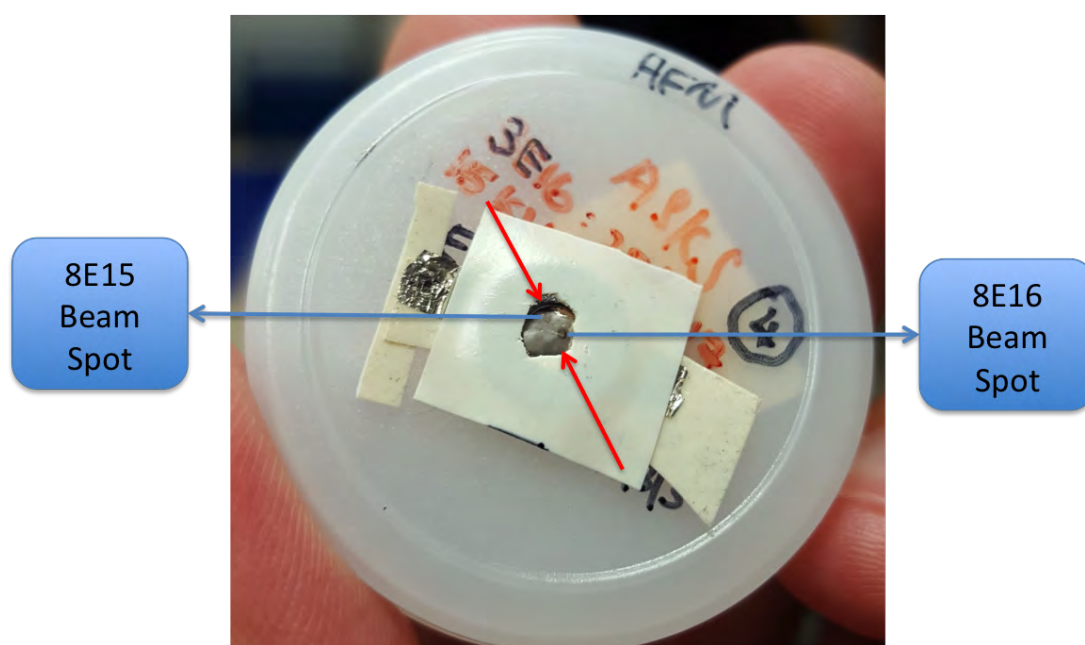
Figure 5.9: Mask-Mounting Method 4 - This mask itself was used 3 times, as can be seen from the 3 beam spots. One was used for testing, and the other 2 used for the stated doses as labelled.

5.2   Main Discussion

A thorough analysis of all the above results is given in this section.

At A Glance					
Dose/ ions cm^2	Mask Method	Pictorial	Approximate Distance of Mask from Substrate/um	Extent of Deposition (in "holes")	Depth of structures/nm
3E16	1		350	Covered with Ni	- 230 ± 20
3E17	1		350	Covered with Ni	- 380 ± 10
3E15	2		180	Some Ni	2.6 ± 2.8
3E16	2		45	SS with Ni boarder	140 ± 10
3E17	3		90	SS with Ni boarder	19.8 ± 0.9
8E15	4		50	SS with Ni boarder	4.5 ± 0.6
8E16	4		200	Covered with Ni	8.1 ± 0.8

Figure 5.10: At A Glance - Useful parameters are detailed in the table above. Note however that each dose used a completely different mask except for 3E16, 3E17 Mask Method 1 and 8E15 8E16 Mask Method 4 which used the exact same mask.

5.2.0.1 Height of Mask above SS

Firstly, the height of each mask was studied in detail using an optical microscope at 100x magnification. This method works by first focusing the microscope on one end of the Ni mask. The Ni mask was then moved along an axis across the centre of the mask, with small step sizes and the optical microscope refocused by adjusting the height of the stage accordingly. Suppose that the height of the stage has to be increased by 10 μm at its new position - this means that this mask position is 10 μm lower than the previous position, given that the focal length of the lens remains the same. Naturally, the highest stage height corresponded to the lowest mask region, and this was set as our reference point, from which the rest of the mask relative height was determined.
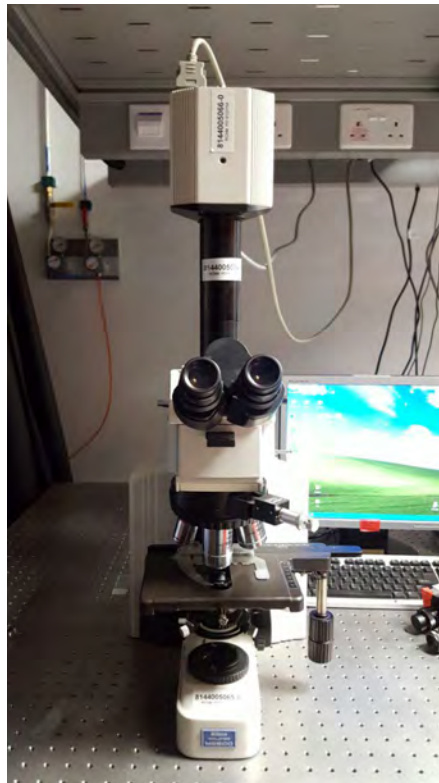

Figure 5.11: Optical Microscope - Has up to 100x magnification and is capable of looking at features that are submicron

An example of this is shown in the table **see above** for mask-mounting method 3, which was used to obtain 3E17 ions cm^{-2} sample. Converting the raw data into

Mask Conformity		
y axis/mm	Height of stage/um	Height of mask/um
100.3	150.0	14.5
100.4	136.0	28.5
100.6	100.5	64.0
100.7	95.0	69.5
100.8	84.5	80.0
101.0	79.0	85.5
101.1	77.0	87.5
101.3	73.0	91.5
101.5	71.5	93.0
101.7	71.5	93.0
101.8	71.0	93.5
101.9	71.5	93.0
102.0	73.0	91.5
102.2	72.0	92.5
102.4	75.0	89.5
102.7	82.0	82.5
102.9	108.5	56.0
103.1	126.0	38.5
103.2	143.0	21.5
103.4	164.5	0.0

Figure 5.12: Mask Profile - Table showing the results using optical microscope focus at 100x magnification, accurate to a resolution of 0.5 um

a graphical figure could help one to better envision the conformality of the mask used.
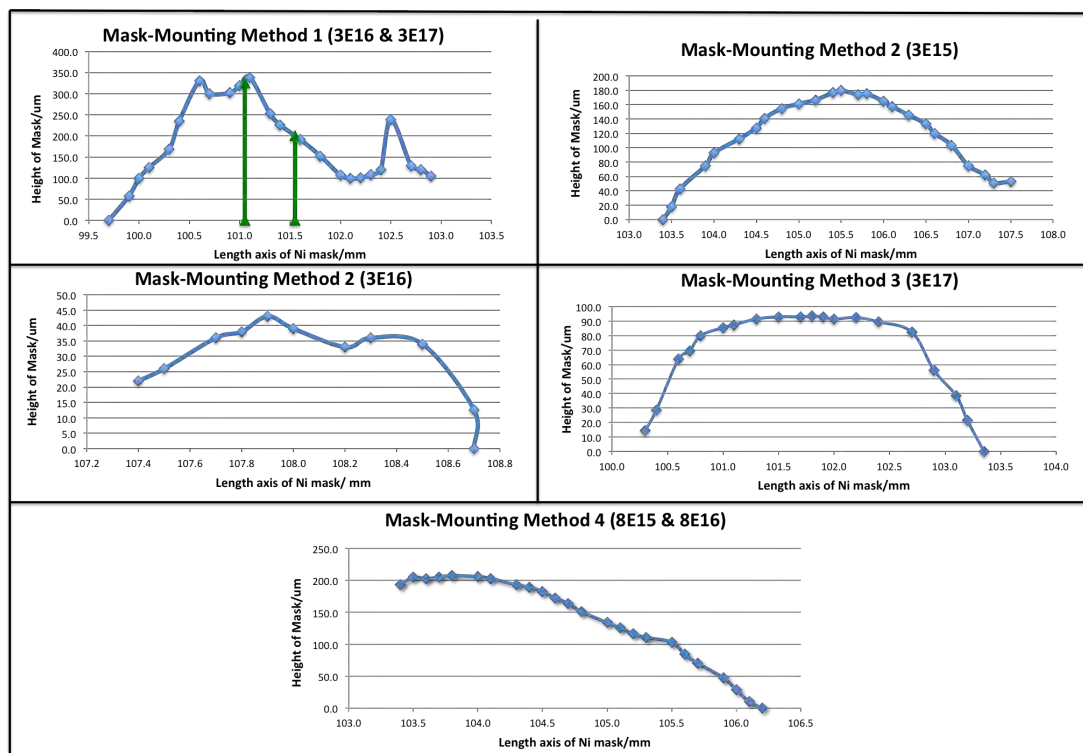

Figure 5.13: Mask Conformity - Showing the pictorial results of various Ni mask used based on information from optical microscope focus at 100x magnification, accurate to a resolution of 0.5 μm

It is important to note that even though zero height represent regions where the mask disappears under the tape (call these regions end points), they cannot be assumed to have truly zero distance from SS surface. This is because the SS surface could have some form of unconfomality in itself which can affect the mask conformality at localised regions especially if the mask is creased at these regions. Furthermore, mask-mounting methods 3 & 4 could also have non conformal contact between the washer and the SS, possibly leading to non conformal mask to substrate distances.

Nevertheless, these end points have distances that are likely to be small compared to the disconformality throughout the Ni mask, and hence it is still rea-

sonable to approximate the height of the mask relative to its "end points" as the actual mask to substrate distance or at least as its lower limit.

From **Figure 5.9**, it is apparent that the distance of the mask from the SS surface does affect the extent of deposition obtained in our structures. It appears that beyond a distance of 180 μm and above, deposition effects become significant. This phenomena increases starkly with distance of mask from substrate as can be observed when we compare the two 3E17 ions cm^{-2} doses. The main difference between these 2 doses lie with the mask distance from the substrate. The one that had a much larger distance (350 μm) from the substrate showed relatively significant **heightened** structures of 400 nm, while the one which had a smaller mask to substrate gap showed 30 nm **depth** in its structures.

Of course, one may rightly point out that the mask profile taken using the optical microscope is about 3mm in diameter, whereas the beam diameter was only 0.5 mm in diameter. In other words, the beam need not have passed through regions on the mask that have the highest mask to substrate distance. As such, the various physical masks used were studied and the beam spots marked by Ar beam exposure were mostly found close to the centre of each mask with the exception of mask-mounting method 4, which was used for the doses 8E15 ions cm^{-2} and 8E16 ions cm^{-2} and had beam spots that were close to the edge.

The mask conformity profiles were then inspected once again, and it is evident that the mask to substrate distance at the centre of these masks were either the maximum or close to the maximum with the exception of mask-mounting methods 1 and 4. For mask 1, a centralised beam spot (marked out by the 2 green vertical lines) would lie at a distance of at least 200 μm away from the substrate. For mask 4, two doses - namely 8E15 ions cm^{-2} and 8E16 ions cm^{-2} were taken on the very same mask, albeit at different and non-overlapping regions of the mask. **Figure 5.9** clearly shows the beam spots belonging to the corresponding doses, and the arrows indicate the axis along which the mask was analysed. Evidently the beam spot for 8E15 ions cm^{-2} lay on a relatively region with shorter mask to substrate distance of about 50 μm whereas the 8E16 ions cm^{-2} lay on a relatively region with relatively further mask to substrate distance of 200 μm. The former is also noted to have experienced little Ni deposition except around the boarders of the holes, whereas the latter was found with Ni material fully covering its holes.

If all the corrected mask to substrate distance (at the centre points of mask 1, 2 & 3 and the corresponding positions based on the beam spots seen for mask 4) were used instead, similar conclusion can still be made - Ni mask deposition effect seems to be significant and clearly observable when the mask to substrate distance is above 180 μm.

5.2.1 Depth of structures vs Dose

The depth of structures vs dose was also investigated in detail. The figure below shows the average depth of structures obtained vs the dose used.

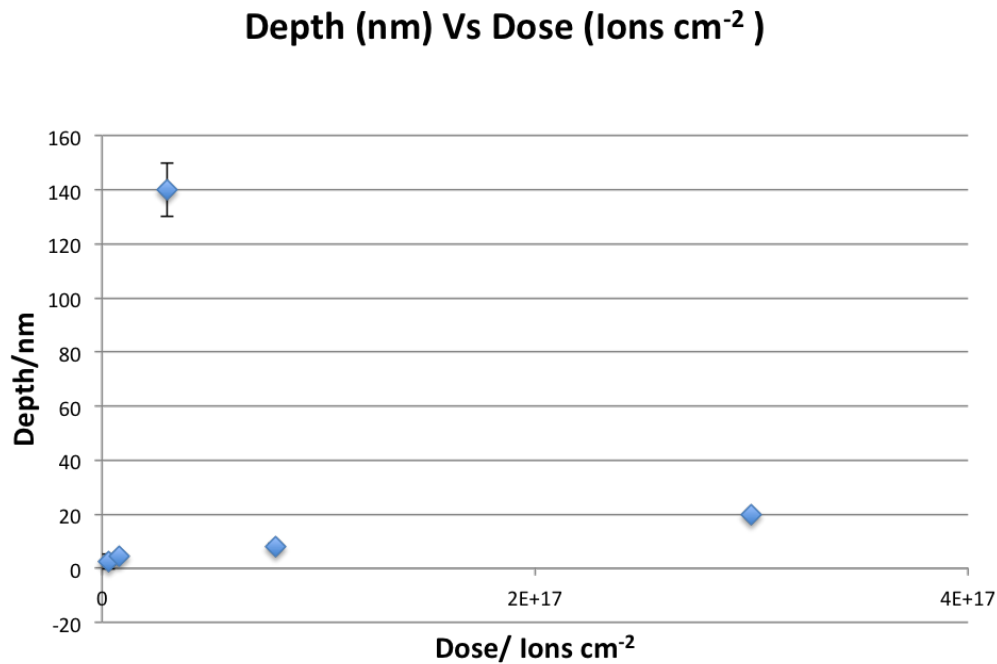**Figure 5.14: Graph of Depth/nm Vs Dose/ions cm^{-2}** - For various doses. Note that 3E16 & 3E17 ions cm^{-2} obtained from mask-mounting method 1 were omitted because they had heightened structures

From the doses of 3E15 to 3E16 ions cm^{-2}, there is an increase in the depth of structures obtained as dose increased, but this trend seemed to reverse when dose was increased beyond 3E16 ions cm^{-2}.

An positive correlation is expected between the depth of "holes" obtained and dose used. Because dose = no. of incoming ions/unit area of target, it is indicative of the number of Ar^+ ions fired per unit area of exposed SS surface. Each time Ar^+ ions hits the SS surface, there is a chance that some SS atoms would be sputtered off. Hence a higher dose implies more ions hitting each unit area of the SS and given the same chance of sputtering by each argon ion, a higher ion dose would increase the sputtering depth.

Yet, after the dose of 3E16 ions cm^{-2}, the trend seems to contradict what was just established. In particular, both the 8E16 and 3E17 doses revealed lower structures than the 3E16 dose. This could possibly be explained because of the redeposition effect. Redeposition effect refers to the phenomena in which sputtered particles fill back the volume in the target from which they were sputtered off. This phenomena is mentioned in some papers, and has been shown to be of a non-linear effect[22][23]. Redeoposition effect depends on a variety of factors like aspect ratio of structures, the depth of structures etc, and hence has no fixed theory or formula to simply apply to our case.

Nevertheless, while this effect could explain why 8E16 & 3E17 doses yielded lower structures as compared to 3E16 dose, it does not explain why 8E16 dose should have a lower structure as compared to 3E17 dose when we expect a higher dose to perhaps increase the significance of redepositon effect.

The reason is, however, linked to what we have discussed earlier - the effects of mask to substrate distance is also at play here, and cannot be ignored, especially so for the 8E16 dose. This is because the phase profile image of 8E16 dose clearly reveals that the surface of the "holes" are completely covered with Ni material, suggesting a high mask-deposition effect, associated with the high mask to substrate distance of 200 μm. On the other hand, the phase images of other doses showed "holes" with at most nickel delineating the boarders. Note that this does not imply that mask-deposition effect did not occur in these experiments, but rather, there is good reason to believe that the mask deposition effect is not significant enough to dominate the sputtering effect in these cases, possibly because they have a much lower mask to substrate distance.

Because 8E16 dose has been found to have significant Ni coverage in its "holes", this implies that its actual depth should have been larger - the Ni layer

not only adds to its height (or reduces its depth), it also hinders the ability of Ar ions to further sputter SS material from the surface. As such, in reality, the 8E16 depth could have been considerably higher than what was obtained and this could have been 1 possibility of how the depth vs dose graph could have looked.
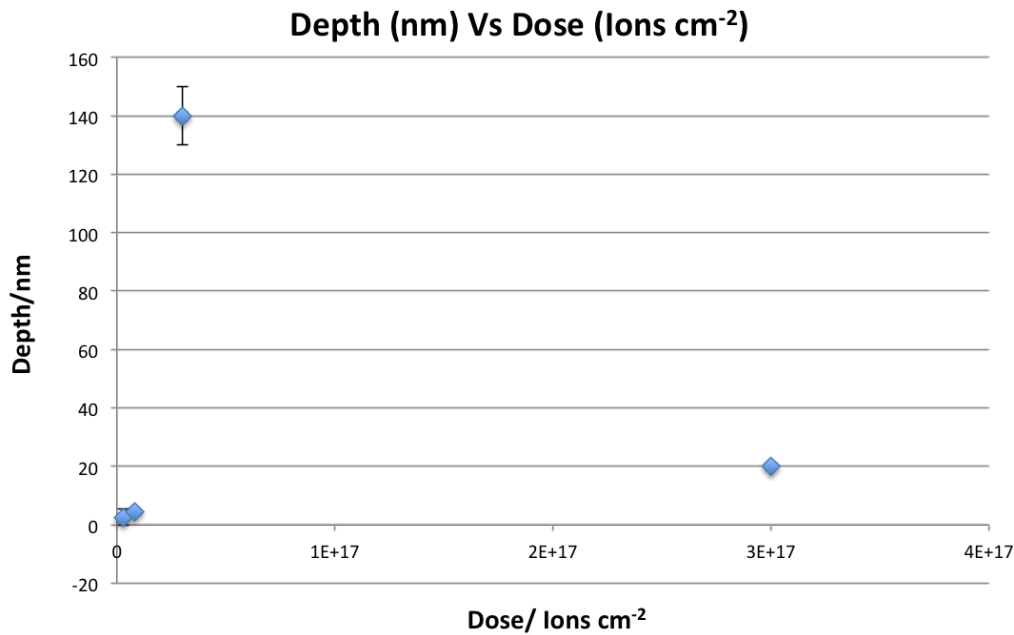

Figure 5.15: Graph of Depth/nm Vs Dose/ions cm^{-2} - For various doses, now omitting 8E16 dose due to significant Ni mask deposition effects. Note that 3E16 & 3E17 ions cm^{-2} obtained from mask-mounting method 1 were omitted because they had heightened structures

5.3 Phase 1 Overall Analysis

Through these experiments, it is shown that there are possibly 3 different factors which come into play when we consider the depth of structures created on a substrate through ion beam lithography via a mask.

(1) Dose - For low dose regimes (in our case probably below 3E16 ions cm^{-2}, increasing the dose should increase the depth of our structures.

(2) However as dose increases beyond a certain threshold, effects of redeposition could occur, and this effect could hinder the sputtering rate and depth. However, too little information is available at this point in time to properly characterise and quantify the extent of this effect.

(3) Mask Material Deposition - This effect was investigated with the help of the AFM phase profile images, and is closely linked to mask-substrate separation. Generally, the higher the separation, the more significant mask deposition becomes and this effect clearly dominates sputtering effects when separation of mask to substrate are above 180 μm.

It is also interesting to note that the uniformity of structures obtained is in some ways linked to the dose. At a dose of 3E15 ions cm^{-2}, the surface of stainless steel that was sputtered showed very rough and discontinuous surface morphology. Even the Ni that was deposited from the mask (due to significant mask to substrate distance), could be seen to be very irregular. This may seem like an "ugly" result but it is actually a beautiful display of the statistical nature of sputtering. When Ar ions hit the surface, sputtering does not happen for certain, but is actually associated with a certain probability. As probability becomes less meaningful at small sample sizes and more "certain" with larger sample sizes - so it is with sputtering. The 3E15 dose happens to be a dose whereby the power of statistics is shaken because the dose is too small. At this dose, there are insufficient incoming ions to ensure that every exposed SS area will be sputtered. Hence, we observe very different localised morphologies. It is only at higher doses of at least 8E15 or 3E16 onwards, where the no. of incoming ions are sufficient to lend strength to to the probability of sputtering, which seems to gain some form of "certainty" as are depicted by regular squarish structures that showcase more uniform extent of sputtering has occured.

5.3.0.1 Further Improvement 2

In phase 1, the effects of mask to substrate separation on the depth of structures obtained have been shown. It was apparent that more could be done to further improve this issue by further minimising this separation and keeping it at a fixed value, so that the effects of redeposition and dose on depth of structures could be more conclusively studied.

However, there is no absolute way of actually monitoring the mask to substrate distance. Our method using a optical microscope was indicative of the lower limit of this distance with the assumptions that the end points of the masks were of negligible distance from the substrate. While this seemed true most of the time, the mask profile of method 4 suggests that this is not always the case. It is also physically strenuous and cumbersome to obtain the mask profile of every mask used, and even more challenging to ensure that the mask to substrate distance is kept constant through mask mounting procedures. Many mask-mounting methods have been tried, including attaching neodymium magnets below the stainless steel surface to pull Ni grid more tightly to it, new methods of taping etc, but these proved to be unfruitful. In the case of neodymium magnets, only a small one could be used, given the small sample holder size in the ISTB. The imperfectly uniform field of the neodymium magnet causes Ni mask to be tightly pressed onto SS at small localised regions, while other parts stood up, creating a very uneven surface. Mask-mounting improvement process is an uphill battle, not only because the Ni mask is extremely fragile but also because new ideas must be fulfilled within the constraints of our machines.

5.4 Phase 2

Phase 2 of this project was aimed at fixing the mask to substrate distance so that it is no longer a variable we have to consider. It was also decided that effort spent on securing a fool-proof mask-mounting method would be an uphill and perhaps unfruitful venture. Hence, an endeavour was made to create and grow a removable mask directly onto the SS surface. This method is expected to vastly minimise the mask to substrate separation.

In phase 1, however, the Ni mask was assessed to be of uniform thickness throughout. As such, mask to substrate separation translates effectively to the height of mask above the SS. It is too early to pin-point whether it is the mask to substrate separation or the height of mask above a surface that truly influences the probability of mask material deposition. As such, the challenge is to strive towards creating a mask that was of conformal height with structures regular in pattern and high in resolution.

Method 1 as introduced in the "Procedures" section was chosen for mask fabrication. An optical image of the grid directly on stainless steel is shown below:

Figure 5.16 depicts the results obtained from the first attempt to create mask directly onto SS. The patterns were made to be similar to Ni mask used in Phase 1, and have turned out to be of similar dimensions and of good resolution. However, small regular defects exist in each of the "holes" which also contain Cr and Cu in some of its localised regions. Nevertheless, because the Cr and Cu appears uniformly throughout all of these holes, there is reason to think that the sputtering process works to a high and consistent resolution. An error in the UV lithography process or in the developing of the Cr mask for UV lithography is suspected to have given rise to such defects. Nevertheless, this result gives us good reason to continue working in this direction.
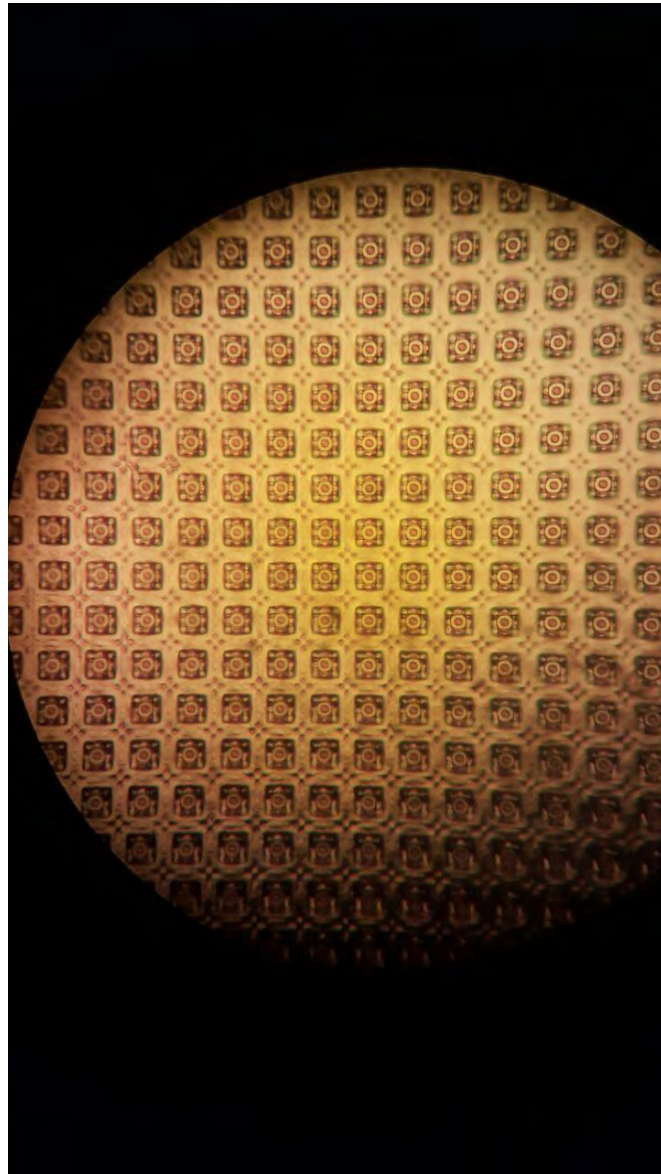
Figure 5.16: Self-Made Mask directly on Stainless Steel - Pattern is similar to Ni mask used in phase 1 so that closer comparisons can be made. The grids are coated with 10 nm of Cr and 500 nm of Cu. However, small defects can be seen in the 6 μm by 6 μm hole structures which have also been deposited uniformly with Cr and Cu at regular regions.

6

Conclusion

In phase 1, characterisation of nano-structures created in stainless steel through the use of Ni-masked ion beam sputtering was investigated. The depth of these structures were found to have a non-linear relationship with the dose used due to redeposition effects coming into play at higher doses (beyond 3E16 ions cm^{-2}). Nevertheless, it was established that 2 dose regimes exist - the low dose regime and the high dose regime. In the low dose regime, the depth of structures created increases as dose is increased. However in the high dose regime, redeposition effect becomes dominant over sputtering effect, and an increase in dose may actually stagnate or decrease the depth of sputtered structures. Also, mask to substrate separation was found to be a vital factor which affected the depth of structures created. Mask material deposited into sputtered structures is a phenomenon that appears dominant if the mask to substrate separation exceeded 180 μm and seemed to be suppressed sufficiently when it was less than 100 μm.

In Phase 2, the challenge was to investigate the non-trivial redeposition effect which can only be conclusively studied by first minimising mask to substrate separation to quench mask deposition effect. This was done by directly growing grids onto stainless steel, which was a process that opened up the opportunity to master at least 4 new machines, 1 new software and various new processes within a short span of time. Nevertheless, the endeavour to grow a mask directly onto SS was a successful one, but this project is still a work in progress, and no conclusive results concerning redeposition effect has been established.

In my research endeavours during this project, I have had the chance of operating and mastering the Ion Sputtering Test Bench (ISTB), spin coater, ultrasound cleaning system, sputtering deposition machine, UV lithography, laser writer, ovens, optical microscopes, AFM, Autocad software, SRIM simulations, various etching processes and more. It was indeed a fulfilling research journey where a steep learning curve was present throughout. Nevertheless, I thank my mentors and colleagues for guiding and trusting me with much research freedom, such that I was enriched with experience not confined simply to theories nor this report, but to utilising and troubleshooting machines, which comes as a good learning opportunity for a physicist to understand how far theories can either give direction to experimental work or be given direction through experimental work.

References

[1] MARIEKE BURGHOORN, DORRIT ROOSEN-MELSEN, JORIS DE RIET, SAMI SABIK, ZEGER VROON, IRYNA YAKIMETS, AND PASCAL BUSKENS. **Single layer broadband anti-reflective coatings for plastic substrates produced by full wafer and roll-to-roll step-and-flash nano-imprint lithography**. *Materials*, **6**(9):3710–3726, 2013. 1

[2] M SINGH, S SINGH, S PRASAD, AND I S GAMBHIR. **Nanotechnology in Medicine and Antibacterial Effect of**. *Digest Journal of Nanomaterials and Biostructure*, **3**(3):115 – 122, 2008. 1

[3] MANN. **Nanotechnology and Construction**. *Institute of Nanotechnology European Nanotechnology Gateway*, (November):2–56, 2006. 1

[4] JASON VALENTINE, JENSEN LI, THOMAS ZENTGRAF, GUY BARTAL, AND XIANG ZHANG. **An optical cloak made of dielectrics**. *Nature Materials*, **8**(7):568–571, 2009. 1

[5] A.P.S. SAWHNEY, B. CONDON, K.V. SINGH, S.S. PANG, G. LI, AND D. HUI. **Modern Applications of Nanotechnology in Textiles**. *Textile Research Journal*, **78**(8):731–739, 2008. 1

[6] DUNCAN SUTHERLAND AND LUISA FILIPPONI. **Fabrication Methods**. *NanoYou - Teachers Training Kit in Nanoscience and Nanotechnologies*, (January):1–21, 2010. 1

[7] HELMUT SCHIFT. **Nanoimprint lithography: An old story in modern times? A review**. *Journal of Vacuum Science & Technology B: Microelectronics and Nanometer Structures*, **26**(2):458, 2008. 2, 4, 5

[8] Nazrin Kooy, Khairudin Mohamed, Lee Tze Pin, and Ooi Su Guan. **A review of roll-to-roll nanoimprint lithography.** *Nanoscale research letters*, **9**(1):320, 2014. 2

[9] B Kwon and Jong H Kim. **Importance of Molds for Nanoimprint Lithography : Hard , Soft , and Hybrid Molds. 2016**, 2016. 2, 4

[10] **Properties of Stainless Steel -grade 304 by Azom @ Www.Heraeus.Com, accessed April 2017**. 4

[11] **Properties of Silicon by MEMSnet @ www.memsnet.org, accessed April 2017**. 4

[12] Helmut Schift and Anders Kristensen. **Nanoimprint Lithography**. *Springer Handbook of Nanotechnology*, (February 2010):239–2786, 2007. 5, 6

[13] Arcelor Mittal. **Stainless Steel and Corrosion**. *Stainless Europe*, page 6, 2010. 5

[14] U. Fano, a. R. P. Rau, and John S. Briggs. **Atomic Collisions and Spectra**. *Physics Today*, **41**(11):120, 1988. 10

[15] Martina Schulte-Borchers. **Proton beam writing**. **10**(6):20–29, 2009. 12

[16] MZ Hossain. **Ion impact energy distribution and sputtering of Si and Ge**. *Journal of Applied . . .* , **103513**:1–6, 2012. 12

[17] **SPI Supplies - Ni fine 5 um mesh @ www.2spi.com, accessed on March 2017**. 14

[18] Nannan Liu, P. Santhana Raman, Xinxin Xu, Huei Ming Tan, Anjam Khursheed, and Jeroen a. van Kan. **Development of ion sources: Towards high brightness for proton beam writing applications**. *Nuclear Instruments and Methods in Physics Research Section B: Beam Interactions with Materials and Atoms*, pages 1–6, 2015. 22

[19] Pang Rudy. **Fabrication and Characterization of Nano Aperture Ion Source For High Brightness Proton Beam Writing**. page 61, 2015. 22

[20] **Advanced Surface Microscopy - Phase Image @ www.asmicro.com, accessed on March 2017**. 31

REFERENCES

[21] J. L. Bartelt, C. W. Slayman, J. E. Wood, J. Y. Chen, C. M. McKenna, C. P. Minning, J. F. Coakley, R. E. Holman, and C. M. Perrygo. **Masked ionbeam lithography: A feasibility demonstration for submicrometer device fabrication**. *Journal of Vacuum Science and Technology*, **19**(4):1166–1171, 1981. 32

[22] R. Mark Bradley. **Redeposition of sputtered material is a nonlinear effect**. *Phys. Rev. B*, **83**:075404, Feb 2011. 45

[23] Henry Holland-moritz, Sebastian Scheeler, Christoph Stanglmair, Andreas Johannes, Henry Holland-moritz, Carsten Ronning, Heungbae Kim, Gerhard Hobler, and Andreas Steiger. **Sputtering and redeposition of ion irradiated Au nanoparticle arrays : direct comparison of simulations to experiments**. 45